Running title: Dissolution of carbonate sediments under rising pCO_2

Dissolution of carbonate sediments under rising pCO_2 and ocean acidification: observations from Devil's Hole, Bermuda

ANDREAS J. ANDERSSON[1*], NICHOLAS R. BATES[1] AND FRED T. MACKENZIE[2]

[1]Bermuda Institute of Ocean Sciences, 17 Biological Lane, Ferry Reach, St. George's GE01, Bermuda

[2]Department of Oceanography, School of Ocean and Earth Science and Technology, University of Hawaii, 1000 Pope Rd, Honolulu, HI 96822

*Author to whom correspondence should be addressed
E-mail: andreas.andersson@bios.edu
Ph. (441) 297 1880 x210; Fax. (441) 297 8143

ABSTRACT

Rising atmospheric pCO_2 and ocean acidification originating from human activities could result in increased dissolution of metastable carbonate minerals in shallow water marine sediments. In the present study, *in situ* dissolution of carbonate sediments in Devil's Hole, Bermuda, was observed during summer when thermally driven density stratification restricted mixing between the bottom water and the surface mixed layer and microbial decomposition of organic matter in the hypolimnion produced pCO_2 levels similar to or higher than those levels anticipated by the end of the 21st century. Trends in both seawater chemistry and sediment composition of Devil's Hole indicate that Mg-calcite minerals are subject to selective dissolution under conditions of elevated pCO_2. The derived rates of dissolution based on observed changes in excess alkalinity and vertical eddy diffusion ranged from 0.3 to 1.6 mmol m^{-2} h^{-1}. On a yearly basis, this range corresponds to 264 to 1402 grams m^{-2} yr^{-1}; the latter rate is close to estimates of the average global coral reef calcification rate of about 1500 grams m^{-2} yr^{-1}. Considering a reduction in marine calcification of 40% by the year 2100, or 90% by 2300 as a result of surface ocean acidification, the combination of high rates of carbonate dissolution and reduced rates of calcification implies that coral reefs and other carbonate sediment environments within the next centuries could be subject to a net loss in carbonate material as a result of increasing pCO_2 arising from burning of fossil fuels.

1. INTRODUCTION

Since the onset of the industrial revolution, the global oceans have served as a significant sink of anthropogenic CO_2 (e.g. Mackenzie et al. 2001; Sabine et al. 2004) that has led to an increase in the surface seawater dissolved inorganic carbon content, pCO_2, and a decrease in pH (ocean acidification). Rising pCO_2 and ocean acidification have produced a decrease in the surface seawater saturation state with respect to calcium carbonate minerals (Kleypas et al. 1999; Feely et al. 2004; Andersson et al. 2005; Orr et al. 2005). Future carbon cycle projections suggest seawater carbonate saturation state will continue to decrease into the future (e.g. Kleypas et al. 1999; Andersson et al. 2005; Orr et al. 2005). As a consequence, marine calcareous organisms may have difficulty calcifying and producing their shells, tests, and skeletons at their historical rates (e.g. Gattuso et al. 1999; Langdon et al. 2000; Riebesell et al. 2000). It is not certain what the ecological consequences of slower calcification and growth rates will be, but other aspects of the marine carbonate community such as reproduction (Rodgers et al. *submitted*), recruitment success (Agegian 1985; Kuffner et al. *in preparation*) and the physical strength of individual calcifying organisms, as well as the carbonate structure itself (e.g. reefs), may be negatively affected by elevated pCO_2 and lower carbonate saturation state, yielding marine calcifying organisms that are less competitive and more vulnerable to environmental stress in general (e.g. Kleypas et al. 1999, 2001, 2006; Andersson et al. 2005).

Decreasing surface seawater carbonate saturation state may also result in increased dissolution of carbonate minerals in shallow water sediments. Preferentially, metastable carbonate phases such as high Mg-calcite of variable Mg content are the first phases to dissolve because they are more soluble than both calcite and aragonite. Such selective dissolution based on mineral stability has been demonstrated in laboratory and field experiments (Wollast et al.

1980; Balzer and Wefer 1980; Walter and Burton 1990) and inferred from carbonate sediment, mineralogy, and petrology observed in natural environments (Chave 1962; Schmalz and Chave 1963; Neumann 1965; Alexandersson 1976, 1979). Because carbonate dissolution produces alkalinity and increases the capacity of seawater to absorb anthropogenic CO_2, knowledge of this process is of great importance in order to understand: 1) the rate and amount at which atmospheric CO_2 is taken up by the oceans (Garrels and Mackenzie 1980; Balzer and Wefer 1981), 2) the rate at which surface seawater chemistry is changing owing to absorption of anthropogenic CO_2, 3) whether carbonate dissolution can act as a buffer to alleviate changes in seawater pH and carbonate saturation state imposed by rising pCO_2, and 4) how carbonate sediment composition will change owing to future changes in seawater chemistry. Hypothetically, if the rate of dissolution of metastable carbonate minerals were to balance the oceanic uptake of anthropogenic CO_2, total DIC and total alkalinity would increase, but there would be little or no net change in pH and carbonate saturation state owing to this process. Consequently, the rate at which marine calcifying organisms calcify would remain unchanged under these conditions (Andersson et al. 2003, 2005; Morse et al. 2006).

The general objective of the present study was to investigate the behavior and reactivity of carbonate minerals under conditions of elevated pCO_2 in a natural environment. Specifically we aimed to determine whether carbonate minerals rapidly respond and dissolve as a result of elevated pCO_2, what carbonate phases are dissolving, how rapidly do they dissolve, does carbonate dissolution add sufficient alkalinity to the surrounding seawater in order to buffer significantly the carbonic acid system, and what does the overall ocean acidification imply in terms of how marine calcifying organisms will be affected in the future owing to rising atmospheric CO_2?

In order to accomplish these objectives we investigated changes in surface seawater chemistry in Devil's Hole, Bermuda, which during summer develops pCO_2 levels similar or higher than those anticipated in the atmosphere within the next centuries as a result of anthropogenic activities.

2. REGIONAL DESCRIPTION

Devil's Hole is located in the southeast corner of Harrington Sound, Bermuda, and is the deepest part of the sound (~24 m) (Figure 1). The sound covers an area of ~4.8 km^2 and has a mean depth of 14.5 m. Water exchange between Harrington Sound and the North Lagoon is driven by tidal movements through Flats inlet, a narrow opening in the southwest corner and the only open entrance to the Sound, but the tidal range of 0.2 m is equally influenced by flow through subterranean channels in the surrounding cavernous carbonate land mass (Morris et al., 1977). Based on the average depth of Harrington Sound, the nominal residence time is close to 30 days with respect to the semidiurnal tidal flow, but effective tidal mixing can be four times as long (Brown 1978, 1980). During late spring or early summer, thermally induced density stratification is developed in the water column throughout Harrington Sound owing to the exponential decrease in absorption of solar irradiance with depth (Brown 1980). Vertical mixing is impeded by this stable density stratification, which isolates the deeper parts (the hypolimnion) of the Sound from the overlying mixed layer (the epilimnion) to a certain extent. As a consequence, organic matter that settles through the water column is remineralized below the thermocline and drives the pCO_2 of the subthermocline region or the hypolimnion to levels much higher than we normally observe in other natural shallow surface seawater environments (Figure 2). Because the sediments are completely dominated by carbonate minerals of varying

composition originating from marine calcifying organisms present within the Sound (e.g., corals, coralline algae, barnacles, holothurians, benthic foraminifera, bryozoans, echinoids etc) or from limestone rocks and eolianites surrounding the Sound, Harrington Sound and Devil's Hole can serve as a natural laboratory to study the behavior of carbonate minerals under elevated pCO_2.

3. METHODOLOGY

3.1 Fieldwork and laboratory analyses

Several day cruises were conducted to Devil's Hole during the summer of 2004 and 2005. Seawater was collected from multiple depths using a single 5 L niskin bottle. For each sampling time, sub-samples of the water from the Niskin bottle were collected and subsequently analyzed for dissolved oxygen (DO), dissolved inorganic carbon (DIC), total alkalinity (TA), and salinity. On a few occasions, samples for total calcium concentration and H_2S were also collected. Dissolved oxygen samples were immediately drawn into 115-ml BOD flasks and fixed with Winkler reagents to avoid atmospheric gas exchange. The temperature of the seawater in the bottom of the Niskin bottle was recorded at this time. Seawater dissolved oxygen was determined by automatic Winkler titrations based on a UV endpoint detector system according to the procedures used by the Bermuda Atlantic Time Series program (BATS; e.g. Knap et al. 1993, 1997). The mean difference between pairs of replicates was ~1.14 μmol kg^{-1} (n=5). Samples for dissolved inorganic carbon and total alkalinity were drawn immediately after DO samples into 200 ml Kimax brand glass sample bottles and poisoned with a saturated solution of mercuric chloride ($HgCl_2$; 100μL). Each bottleneck was prior to sampling taped with teflon tape to assure a tight seal to prevent atmospheric equilibration. DIC content was analyzed using an infrared DIC analyzer employing a Li-Cor 6262 NDIR analyzer as detector (for details, see

http://www.bbsr.edu/Labs/co2lab/research/CO2_instrumentation.html). The 1σ precision of total DIC was 0.13% (~2.64 μmol kg^{-1}; n=30). TA was determined by potentiometric acid titrations (DOE, 1994) similar to the procedure described by Bates et al. (1996). The 1σ precision of TA analysis was 0.075% (~1.70 μmol kg^{-1}; n=12). Both DIC and TA were determined relative to certified reference material (CRM) prepared by Andrew Dickson at Scripps Institution of Oceanography. Seawater for salinity determination was drawn into salinity glass bottles and analyzed by an autosalinometer according to the BATS protocol (e.g. Knap et al. 1993, 1997). Calcium samples were drawn and stored in 40 or 60 ml amber plastic bottles. Complexometric titration with EGTA based on potentiometric endpoint detection was used for calcium determination (Kanamori and Ikegami 1980), and was standardized with $CaCl_2$ standard solution from Fisher Scientific. The mean 1σ presicion on triplicate analyses was 0.30% (~33 μmol kg^{-1}; n=6). On one occasion H_2S samples were collected simultaneously with dissolved oxygen samples when anoxia was suspected. The samples were fixed according to the same protocol as dissolved oxygen samples and analyzed according to the titrimetric method originally proposed by Andersen and Føyn (1969) and described by Fonselius (1983).

3.2 Calculations of carbonate dissolution and vertical eddy diffusion coefficients

3.2.1 Carbonate dissolution

Carbonate mineral dissolution can be inferred from observed anomalies in seawater total alkalinity and calcium concentration normalized to a fixed salinity. Under aerobic conditions and constant salinity, carbonate dissolution and precipitation reactions are the dominant processes affecting total alkalinity in seawater. Photosynthesis and respiration slightly affect total alkalinity because of the associated uptake and release of nutrients, which are part of the minor dissolved constituents that contribute to seawater total alkalinity (e.g. Brewer and Goldman 1976; Dickson,

1981; DOE 1994; Zeebe and Wolf-Gladrow 2003). These changes are in most cases negligible relative to the changes imposed by carbonate dissolution and precipitation. Consequently, under constant salinity, net carbonate mineral dissolution (or precipitation) can be determined from observed changes in seawater total alkalinity, a method most often referred to as the alkalinity anomaly technique (Smith and Kinsey 1978; Chisholm and Gattuso 1991). Under anoxic conditions, microbial reduction of sulfate into sulfide can result in a significant increase in total alkalinity (e.g. Thorstensson and Mackenzie 1974; Morse and Mackenzie 1990). Furthermore, anaerobic decomposition of organic matter generates ammonia (NH_3), which also could significantly contribute to the total alkalinity. Thus, alkalinity changes under anoxic conditions may not only reflect carbonate dissolution, but also microbial sulfate reduction and ammonia production, which may have to be corrected for in order to determine the extent of carbonate dissolution based on changes in total alkalinity. However, regardless of the influence of processes other than carbonate mineral dissolution on total alkalinity, carbonate dissolution can be unequivocally ascertained by considering changes in calcium concentration at a fixed salinity.

In the present study, evidence of carbonate dissolution was obtained from observed anomalies in both total alkalinity and calcium concentration normalized to a salinity of 36, as well as from trends in sediment content and composition based on data from Neumann (1963, 1965), who investigated processes of recent carbonate sedimentation in Harrington Sound. His data have been reevaluated in the present study. As is demonstrated in the results section, changes in total alkalinity agreed well with the extent of carbonate dissolution predicted from changes in calcium concentration. Therefore, rates of carbonate dissolution were calculated by adding the observed rate of change in excess alkalinity between consecutive sampling times to the average calculated rate of vertical diffusion of alkalinity out of the subthermocline layer

during the same time period. Excess alkalinity was estimated by integration of multiple linear regressions fit to the subthermocline alkalinity data (see Appendix). Vertical flux (F) of alkalinity per unit area and unit time was calculated based on Fick's first law of diffusion:

$$F = -D \times \frac{dTA}{dz}, \quad (1)$$

where D is the diffusion coefficient in $m^2\ s^{-1}$ and dTA/dz is the vertical concentration gradient of total alkalinity in the depth range of the thermocline in units of mmol m^{-3} per m. Molecular diffusion was neglected in the current calculations because of its small effect ($D \approx 10^{-9}\ m^2\ s^{-1}$) relative to the effect of turbulent mixing and associated eddy diffusion coefficients ($D \approx 10^{-6}\ m^2\ s^{-1}$).

3.2.2 Vertical eddy diffusion coefficients

Based on changes in water temperature at different depths and times, the vertical eddy diffusion coefficient D(z,t) has been estimated in many lakes from the equation (e.g. Li 1973):

$$F(z,t) = \int_{z}^{z_1} \left(\frac{\partial T(z,t)}{\partial t} \right)_z dz = -D(z,t) \times \left(\frac{\partial T(z,t)}{\partial z} \right)_t, \quad (2)$$

where $F(z,t)$ is the total heat diffused through a unit horizontal area per unit time at depth z and time t, $\partial T/\partial z$ and $\partial T/\partial t$ are the partial differentials or the observed changes in temperature as a function of depth and time, respectively, and z_1 is the depth where $\partial T/\partial t = 0$ or the bottom depth. Equation (2) is only valid under conditions for which: 1) there is no vertical advection of water, 2) the net horizontal heat transport is negligible small, and 3) the heat exchange between water and sediments is small (Li 1973). Brown (1980) concluded that the heat budget for the subthermocline water mass in Harrington Sound, in addition to turbulent mixing, is significantly affected by both sediment conduction and sediment reflection of irradiance as well as downward irradiance. Consequently, direct application of equation (2) to temperature data from Devil's

Hole may erroneously estimate the eddy diffusion coefficients at this location. In order to account for the additional factors significantly contributing to the heat budget in Devil's Hole, careful measurements of both downward and upward irradiance as well as the temperature gradient of the sediment pore water are necessary. Taking these parameters into account and adopting the sediment temperature gradient observed by Thorstenson and Mackenzie (1974), Brown (1980) concluded based on a heat budget balance that the eddy diffusion coefficient of the subthermocline waters of Devil's Hole during the summer of 1979 ranged from 2×10^{-6} to 6×10^{-6} m^2 s^{-1} between 18 and 24 m depth.

Another approach estimates vertical eddy diffusivity based on buoyancy calculations (Denman and Gargett 1983):

$$K_z = 0.25 \in N^{-2}, \quad (3)$$

where K_z is the eddy diffusion coefficient, $\in$ is the turbulent energy dissipation and N is the bouyancy frequency. N is essentially a meaurement of the local stratification and can be calculated from the equation:

$$N^2 = (g/\rho_w)\,(\partial\rho/\partial z), \quad (4)$$

where g is the acceleration due to gravity (9.8 m s^{-2}), ρ_w is density of the water and $\partial\rho/\partial z$ is the vertical density gradient. Using this approach, vertical eddy diffusion coefficients were calculated for each sampling date in Devil's Hole during the summer of 2004 and 2005. The turbulent energy dissipation $\in$ was taken as 2×10^{-8} m^2 s^{-3} based on microstructure measurements in the late summertime thermocline of an open ocean location during conditions of low winds (Dillon and Caldwell 1980; Denman and Gargett 1983). We realize that the turbulent energy dissipation in Devil's Hole may have been different than that of this location, but the calculated

range of eddy diffusion coefficients was similar to the range estimated by Brown (1980) (Table 1); the latter was therefore used in order to calculate a range of vertical alkalinity flux.

3.2.3 CO_2 system parameters

Dissolved inorganic carbon system calculations were calculated at *in situ* temperature and salinity conditions based on total alkalinity and total dissolved inorganic carbon concentration, and stoichiometric carbonic acid system constants defined by Mehrbach et al. (1973) and refit by Dickson and Millero (1987) using the program CO2SYS (Lewis and Wallace 1998).

4. RESULTS

4.1 General physiochemical properties and trends

In August and September of 2004 and 2005, the water temperature of the mixed layer in Devil's Hole remained relatively constant and ranged from 29 to 30 °C (Figure 3). At a depth of 13-18 m, a strong thermocline, which extended all the way to the bottom, was present. The water temperature decreased by 5 to 6 °C in the thermocline. In both years, the depth of the onset of the thermocline migrated downward in the water column over time. Salinity was constant in the mixed layer for each sampling time, but showed differences between consecutive dates. In 2004, the surface layer was less saline than the subthermocline layer, and in 2005, the opposite was observed. The salinity of the hypolimnion was relatively constant for consecutive sampling dates of each year. T-S diagrams confirm these observations and clearly separate the mixed layer from the subthermocline water mass (Figure 4), which also is apparent in density profiles that demonstrate significant stratification (Figure 3). In 2005, T-S properties of the subthermocline water mass more or less conformed to conservative mixing between two end members, i.e. the epilimnion and hypolimnion. The trend was more complex in 2004, indicating very little mixing between the mixed- and subthermocline layers.

Dissolved inorganic carbon (DIC) and total alkalinity (TA) concentrations were constant in the upper mixed layer (Figure 3), but increased significantly in the subthermocline layer. In contrast, dissolved oxygen (DO) rapidly decreased in this layer and the bottom water was observed to be anoxic on a few occasions (Figure 3). Concurrent with anoxic water samples, the presence of hydrogen sulfide was noticed by smell and by the formation of a black precipitate (HgS(s); Goyet et al., 1991) upon addition of $HgCl_2$ (aq) to the DIC-TA samples collected at 23 and 23.5 m on Sep 16, 2004. Similar observations were made on Aug 16 and Sep 6 in 2005 for samples collected at 23.5 m. H_2S analysis of two bottom water samples collected on Sep 14, 2005, yielded an approximate H_2S concentration of 2 μmol kg^{-1} at 23 m, and 46 μmol kg^{-1} at 23.5 m potentially contributing 4 and 92 meq kg^{-1} alkalinity, respectively, at these depths on this date. Similarly, a H_2S concentration of 7 μmol kg^{-1} was observed at 23 m depth in the summer of 1979 (Balzer and Wefer, 1980). The total alkalinity data in Figure 3 reflects the titration alkalinity only and has not been corrected to account for the loss in alkalinity associated with the precipitation of mercuric sulfide (~2 × total sulfur; TS = $[H_2S+HS^-+S^{2-}]$; Goyet et al. 1991). Thus, the *in situ* total alkalinity of anoxic samples in Devil's Hole was actually higher than presented here. Therefore, in any calculations of the carbonate chemistry involving DIC and TA in the present study, samples showing evidence of H_2S were omitted.

Anoxic water samples were associated with a large spike in total alkalinity and DIC content relative to overlying oxygenated water (Figure 3). This spike in alkalinity could reflect the presence of sulfide alkalinity that did not precipitate out on addition of $HgCl_2$ (aq) or ammonia production from decomposition of organic matter. However, based on the H_2S concentrations observed in Devil's Hole, $HgCl_2$ (aq) was added in excess to the water samples collected, and most likely the mercury reacted with the sulfide and removed quantitatively the

alkalinity owing to this constituent. Moreover, according to Morris et al. (1977), ammonium concentrations (NH_4^+) in the hypolimnion waters of Devil's Hole may attain values of 20 μmol kg^{-1}, which are negligble relative to the total titration alkalinity and cannot account for the large alkalinity spike. Thus, it is hypothesized that the large spike and steep gradient in total alkalinity probably reflect the existence of a benthic bottom boundary layer, as observed by Thorstensson and Mackenzie during numerous scuba dives to the bottom of Devil's Hole (F. T. Mackenzie, personal communication). This conclusion is supported by the fact that the DIC data showed a similar gradient.

Following the observed trend in DIC, pCO_2 increased from values slightly higher than equilibrium with the atmosphere (~380 μatm) in the mixed layer to levels ranging from 1000 μatm to close to 2000 μatm at 23 m depth in the subthermocline layer (Figure 5). In contrast to the pCO_2 trend, pH_{tot} decreased from a pH >8 in the upper layer to pH values ranging from ~7.5 to 7.7 at 23 m depth. Seawater saturation states with respect to carbonate minerals decreased in the subthermocline layer reaching values close to equilibrium with aragonite at 23 m depth (Figure 5). Consequently, waters were undersaturated at this depth with respect to Mg-calcite minerals with greater solubility than aragonite and these phases potentially could dissolve.

4.2 Evidence of carbonate dissolution

Calcium concentration in Devil's Hole was constant in the surface mixed layer, but significantly increased with depth in the subthermocline section of the water column (Figure 6). Evaluating calcium concentrations as a function of total alkalinity data (both parameters normalized to S=36 and excluding anoxic samples) collected in the months of September in 1978 (Balzer and Wefer 1981) and 2004, a significant linear relationship between these variables was present during both years. The slope of the combined data sets was equal to 0.42 (r^2=0.80),

which is close to the theoretical slope of 0.5 considering dissolution of a carbonate phase comprised of only Ca^{2+} and CO_3^{2-} ions, such as calcite and aragonite. The close agreement to the theoretical value demonstrates that the influence of sulfate reduction and the production of ammonia and other minor constituents on total alkalinity in the oxic portion of the hypolimnion was negligible. If samples from the anoxic portion were included in the evaluation, the slope was equal to 0.34 (r^2=0.84), which may reflect a minor influence from processes other than carbonate dissolution on total alkalinity, but it could also simply reflect the relatively large variability inherent in the calcium data (Figure 6). However, because the majority of the alkalinity increase is balanced by a corresponding increase in calcium, it can be concluded that the excess alkalinity in Devil's Hole originates mostly from dissolution of carbonate minerals. Furthermore, it is likely that biogenic Mg-calcite minerals that contain a significant percentage $MgCO_3$ (up to 30 mol%; Chave 1954), and are more soluble than both calcite and aragonite (e.g. Bischoff et al. 1987, 1993; Busenberg and Plummer, 1989), are preferentially the first phases to respond to elevated pCO_2 and undergo dissolution (Morse et al. 2006). The observed slope of 0.42 based on the data from the oxic portion of the hypolimnion in Devil's Hole corresponds to dissolution of an average carbonate phase of 16 mol% $MgCO_3$.

4.3 Rates of carbonate dissolution

Rates of carbonate dissolution in Devil's Hole were calculated based on changes in excess alkalinity and the vertical diffusive flux of alkalinity out of the hypolimnion. In 2004, excess alkalinity increased between consecutive sampling days by 0.1 mmol m^{-2} h^{-1}, and in 2005, changes in excess alkalinity ranged from 0.1 to 0.3 mmol m^{-2} h^{-1} (Table 2; Figure 7). The observed changes were close to but somewhat lower than the minimum estimates of vertical diffusion of alkalinity, which ranged from 0.2 to 0.6 mmol m^{-2} h^{-1} calculated based on an eddy

diffusion coefficient of 2×10^{-6} m^2 s^{-1}. The upper estimates of vertical diffusion ranged from 0.5 to 1.8 mmol m^{-2} h^{-1} based on an eddy diffusion coefficient of 6×10^{-6} m^2 s^{-1}. Consequently, in the calculation of carbonate dissolution rates, turbulent diffusion of alkalinity was the more important variable than observed changes in excess alkalinity. Taking both of these parameters into account, the rate of carbonate dissolution in the subthermocline waters of Devil's Hole ranged from 0.3 to 1.6 mmol m^{-2} h^{-1} (Table 2).

4.4 Sediment composition

According to the data of Neumann (1963, 1965), the sediments of Harrington Sound are dominated by aragonite (65 wt%), followed by calcite and low Mg-calcite (<8 mol% $MgCO_3$; 26 wt%), and finally high Mg-calcite (>8 mol% $MgCO_3$; 9 wt%) (Figure 8). Aragonite appears dominant for all grain sizes and at most depths although a decreasing trend is observed from the sand-sized classes to the silts. In this range, the relative abundance of both low Mg-calcite and high Mg-calcite increases. The relative abundances of the different carbonate phases remain relatively constant in the silt to the clay-sized sediment classes. However, a distinct trend of decreasing high Mg-calcite as a function of depth is clearly present in this size range. The difference between shallow and subthermocline sediments is statistically highly significant (Figure 8; ANOVA, $p<0.01$). Furthermore, a decreasing trend in $MgCO_3$ content with depth is observed from the mode mol% $MgCO_3$ of the second calcite peak determined from XRD analysis (Figure 8). This peak represents the higher $MgCO_3$ composition of a sample that has a bimodal Mg-calcite composition.

5. DISCUSSION

The observed increase in pCO_2 owing to microbial decomposition of organic matter and the subsequent decrease in seawater saturation state with respect to carbonate minerals of the subthermocline waters of Devil's Hole may be analogous to the future effects on the global ocean arising from anthropogenic emissions of CO_2 to the atmosphere and absorption of part of this CO_2 in surface ocean waters. The pCO_2 in the bottom waters of Devil's Hole reached levels close to 2000 μatm (Figure 5), which are significantly higher than the pCO_2 of approximately 700 μatm projected for the atmosphere at sea level by the end of the 21st century assuming a business-as-usual emission scenario (IPCC 2001; note that for shallow, well-mixed surface waters with little or no influence from terrestrial input, seawater pCO_2 will not be significantly different from the overlying atmospheric pCO_2). In a similar scenario, the pCO_2 observed in Devil's Hole is close to levels projected for the 23rd century, reflecting maximum atmospheric CO_2 concentrations anticipated from burning of the complete reservoir of conventional fossil fuels (Archer et al. 1998; Caldeira and Wikett 2003; Andersson et al. 2005). An increase in pCO_2 and CO_2 (aq) arising from either organic matter decomposition or atmospheric invasion will react with CO_3^{2-} ions according to the general reaction:

$$CO_2 + H_2O + CO_3^{2-} = 2HCO_3^- \quad (5)$$

As a consequence, the saturation state (Ω_x) with respect to carbonate minerals will decrease because of the consumption of CO_3^{2-} ions:

$$\Omega_x = \frac{[Ca^{2+}]^{1-x} \times [Mg^{2+}]^x \times [CO_3^{2-}]}{K_{sp}^*} \quad (6)$$

where [ ] indicates total concentrations of calcium, magnesium and carbonate ions, respectively, and K_{sp}^* is the stoichiometric solubility product based on ion concentrations. If $\Omega>1$ at *in situ*

conditions with respect to a particular mineral phase, the seawater is said to be supersaturated with respect to that mineral phase and if $\Omega<1$, the seawater is undersaturated. Undersaturation implies that the mineral phase potentially could be subject to net dissolution.

The seawater saturation state of Devil's Hole reached levels close to equilibrium with aragonite (Figure 5), and consequently the seawater was undersaturated with any mineral phase having greater solubility than aragonite. Depending on the Mg-calcite solubility curve adopted, this corresponds to a Mg-calcite phase with greater than ~8 mol% $MgCO_3$ (Plummer and Mackenzie 1974) or ~12 mol% $MgCO_3$ (e.g. Bischoff et al. 1987,1993; Busenberg and Plummer 1989; see Morse et al. 2006 for a detailed discussion of the problems associated with Mg-calcite solubility). Consequently, based on the seawater carbonate saturation states observed in the subthermocline waters of Devil's Hole, Mg-calcite minerals containing a significant mol% $MgCO_3$ are expected to undergo dissolution. Furthermore, the pCO_2 and the carbonate saturation state of the interstitial pore waters of Devil's Hole surface carbonate sediments, which have been carefully characterized by Thorstenson and Mackenzie (1974), were most likely higher and lower, respectively, than what were observed in the water column owing to microbial decomposition of organic matter in the sediments.

As anticipated from the subthermocline seawater carbonate saturation state, calcium data and total alkalinity data unequivocally confirm that dissolution of carbonate minerals indeed is taking place in the subthermocline regions of Harrington Sound. The observed calcium and alkalinity ratios suggest that the average composition of the dissolving phase contains significant mol% $MgCO_3$ (Figure 6). Moreover, despite abundant production of fine-grained high Mg-calcite minerals by *Amphiroa*, *Peyssonelia*, lithothaminoids, holothurians, benthic foraminifera, bryozoans, echinoids and other organisms in the shallow regions of Harrington Sound, there is

little mineralogic evidence for their presence in the fine-grained fractions of the deeper sediments (Neumann 1963, 1965). In addition, a decreasing trend in the relative abundance of high Mg-calcite for the silt- and clay-sized sediment fraction is clearly evident as a function of depth of the surface sediments (Figure 8). The sediment composition at different regions within Harrington Sound is certainly influenced by its source regions, and it could be argued that the observed high Mg-calcite trend of the fine-grained fractions is simply a reflection of this. Neumann (1963, 1965) noticed a distinct depth zonation of major benthic organisms in Harrington Sound and important Mg-calcite producers such as those previously described are very abundant in the shallow parts of the Sound. However, most of these organisms are present only down to a maximum depth range of 10 to 17 m, although echinoids and annelida are abundant within this depth range. Aragonite producing organisms are abundant throughout the depth range from the sea surface to 17 m depth. The zone between 10 and 17 m has been classified as the Oculina zone because of the large abundance of the mud living coral *Oculina valenciennesi* (Neumann 1963, 1965). Below 17 m, no significant calcareous organisms are found, except for one pelecypod species (*Transenella conradina*), which comprises the entire coarse fraction of sediments within this depth zone. In general, there are few calcifying organisms producing hard structures made of calcite or low Mg-calcite. Most of these are planktonic, such as coccolithophorids or foraminifera, but plankton tows in Harrington Sound have not revealed any significant abundance of these organisms (Neumann 1963, 1965). Hence, the majority of low Mg-calcite in the sediments originates from erosion of the surrounding limestone or eolianite. If in fact the observed decreasing trend in relative abundance of fine-grained high Mg-calcite minerals with depth were due to its dispersal from its shallow source regions, the same trend should be observed for low Mg-calcites. This is not the case, and in face

of the abundant supply of high Mg-calcite minerals within Harrington Sound, the only plausible explanation for the paucity of Mg-calcite, and especially the fine-grained biological detritus of these phases, in the subthermocline sediments is selective dissolution (Neumann 1963, 1965), a conclusion also supported by the observed changes in subthermocline seawater chemistry. Furthermore, Balzer and Wefer (1980) demonstrated based on saturometry experiments increasing undersaturation and dissolution of coral (aragonite), oyster (~8 mol% Mg-calcite), and sea urchin (~12 mol% Mg-calcite) as a function of depth in Devil's Hole. These authors also deployed bell jars on the bottom of Devil's Hole and concluded that the majority of carbonate dissolution occurred at the sediment-water interface rather than in the sediments because the release rate of alkalinity of 0.6 mmol m^{-2} h^{-1} could not be supported by the chemical gradient observed in the top 5 cm of the sediments.

In summation, both the subthermocline sediment data and the seawater chemistry data of Devil's Hole agree and unequivocally demonstrate that carbonate sediments are subject to dissolution under conditions of elevated pCO_2. Several lines of evidence suggest that the average composition of the dissolving phase is represented by a high Mg-calcite phase:

(1) Subthermocline seawater is undersaturated with respect to Mg-calcite minerals with a greater solubility than aragonite.

(2) Subthermocline seawater calcium and total alkalinity ratios are less than 0.5.

(3) The relative weight percent of high Mg-calcite decreases with depth of the surface sediments for silt- and clay-sized sediment grains.

(4) The mode mol% $MgCO_3$ of the second calcite peak of surface sediments in Harrington Sound decreases with water column depth.

The results confirm that high Mg-calcite minerals are the first responders to rising pCO_2 and their abundance in contemporary shallow water carbonate sediments could decline due to selective dissolution. Furthermore, Agegian (1985; Mackenzie and Agegian 1989) observed in controlled microcosm experiments that the Mg content of the red algae *Porolithon gardineri* varied linearly as a function of seawater carbonate saturation state. If this trend is true for other calcifying Mg-calcite producers, the average Mg composition of carbonate sediments could also decline owing to decreasing Mg content of the sediment source material originating from shells and skeletons of calcifying organisms.

The calculated range of carbonate dissolution rates in Devil's Hole varies by a factor of five (0.3 to 1.6 mmol m^{-2} h^{-1}). The source of this uncertainty mainly arises from the error associated with the value of the eddy diffusion coefficients and the calculation of the diffusive flux of alkalinity out of the hypolimnion. Changes in excess alkalinity were of the same magnitude as the lower diffusive flux estimate and did not vary significantly between consecutive sampling dates. The estimate of vertical eddy diffusion coefficients by Brown (1980) ranged from 2 m^2 s^{-1} at 18 m depth to 6 m^2 s^{-1} at 24 m depth in the summer of 1979. Assuming this trend is representative of the turbulent conditions of the summers of 2004 and 2005, adopting the higher estimate to calculate the alkalinity flux based on the gradient predominantly observed in the 17 to 21 m depth range may significantly overestimate the actual alkalinity flux. Thus, the lower dissolution estimates for each date may more accurately represent the actual rates of carbonate dissolution in Devil's Hole ranging from 0.3 to 0.7 mmol m^{-2} h^{-1} (Table 2). However, eddy diffusion coefficients calculated for the depth range 17 to 21 m based on the bouyancy method were similar to the upper estimate of Brown (1980) in the summer of 2004, but were closer to the lower estimate in 2005 (Table 1). Taking these differences in eddy

diffusivity into consideration, the range of the derived rates of carbonate dissolution in Devil's Hole ranged from 0.3 to 0.9 mmol m^{-2} h^{-1}. Because of the uncertainty associated with the eddy diffusion coefficients, the minimum estimate of 0.3 mmol m^{-2} h^{-1} and the maximum estimate of 1.6 mmol m^{-2} h^{-1} should be viewed as a lower and an upper bound under the present environmental conditions, respectively. The rate of carbonate dissolution derived from the alkalinity flux into bell jars placed on the bottom of Devil's Hole in the summer of 1979 was equal to ~0.3 mmol m^{-2} h^{-1} (Balzer and Wefer 1980).

Despite the unusual high pCO_2 in Devil's Hole and the large range of the rate of carbonate dissolution derived in the present study, this range is similar to dissolution rates derived from sediments of other tropical and subtropical environments, as well as from experimental setups. In a recent summary based on 15 different settings including both experimental and natural carbonate sediments (Table 3; Kleypas et al. 2006), the derived rate of dissolution of carbonates ranged from 0.1 to 7.0 mmol m^{-2} h^{-1}. The average was 2.3 mmol m^{-2} h^{-1} with a standard deviation of 4.8 mmol m^{-2} h^{-1}. Note that even the upper bound of the present study is significantly lower than this average value, although it should be pointed out that 80% of these data were in the range of 0.1 to 1.5 mmol m^{-2} h^{-1}. Most results were derived based on the alkalinity anomaly technique, measuring alkalinity changes in the water column overlying the benthos either *in situ* (e.g. Barnes and Devereux 1984; Boucher et al. 1998), in field incubation chambers (Halley and Yates 2003, 2006), in experimental mesocosms (Leclercq et al. 2002) or the biosphere 2 (Langdon et al. 2002), making the assumption that the observed changes in alkalinity reflect net carbonate dissolution. Based on a different approach, Walter and Burton (1990) estimated the rate of dissolution for substrates of red algae (18 mol% $MgCO_3$), echinoids (12 mol% $MgCO_3$) and corals (aragonite) submerged in natural carbonate sediments at depths

ranging from 0-30 cm for 1 year. Based on weight loss, the calculated rate of dissolution of the red algae ranged from 0.4 mmol m^{-2} h^{-1} in an area of substantial sea grass cover to 0.8 mmol m^{-2} h^{-1} in an area dominated by mangrove. Neither the echinoid nor the coral substrate showed evidence of dissolution rates as high as the red algae and mass loss of these substrates ranged from 2% to 9% of the dissolved mass of the algae. The observed differences in dissolution rates between substrates were consistent with their mineral composition and reactive surface area (Walter and Burton 1990). Based on vertical gradients in pore water chemistry ($[Ca^{2+}]$ and TA) of carbonate sediments in the Bahamas, Burdige and Zimmerman (2002) determined carbonate dissolution rates as a function of sea grass density. Their estimates ranged from 0.01 mmol m^{-2} h^{-1} in ooithic sands with no sea grass coverage to 0.04 mmol m^{-2} h^{-1} in an area of high sea grass density. The higher dissolution rate in the latter area was attributed to enhanced oxygen transport into the sediments through the roots and rhizosomes of sea grasses driving aerobic decomposition of organic matter and consequently carbonate dissolution owing to the production of CO_2. In summary, estimates of the rate of carbonate dissolution from a wide range of different regions and settings, using different approaches, range by almost three orders of magnitude.

Despite significant differences in the pCO_2 of the water overlying the sediments, the similarity in dissolution rates determined in this study compared to the majority of other studies suggests that the extent of carbonate dissolution is mainly controlled by microbial processes in the pore water-sediment system and at the sediment-water interface rather than the carbonate chemistry of the water overlying the sediments. In favor of this hypothesis, Lecqlerc et al. (2002) concluded based on mesocosm experiments that the pH and carbonate saturation state of interstitial pore-waters were little affected by changes in the surface seawater carbonate

chemistry. Andersson et al. (2005) reached similar conclusions based on numerical simulations using the Shallow-water Ocean Carbonate Model and suggested that the extent of carbonate dissolution is mainly controlled by microbial decomposition of organic matter (e.g., Moulin et al. 1985; Morse and Mackenzie 1990). Consequently, if these conclusions are true, future increases in atmospheric CO_2 and associated changes in surface seawater carbonate saturation state may only have a small effect on the rate of sediment carbonate dissolution. However, although the pCO_2 of the hypolimnion in Devil's Hole was similar or higher to those pCO_2 levels anticipated in the next century, the environmental conditions were not those of a typical coral reef or shelf region. In fact, several aspects suggest that the derived range of carbonate dissolution rates could be significantly underestimated. Primarily, the circulation and mixing of the subthermocline region in Devil's Hole are very limited. Thus, alkalinity produced from carbonate dissolution is allowed to accumulate and to some extent buffer the system. This results in slower rates of carbonate dissolution. In a well-mixed system, the alkalinity increase would be rapidly diluted and carbonate dissolution would proceed at a higher rate, which has been clearly demonstrated by the numerical simulations of Morse et al. (2006). Furthermore, because of the restricted mixing, oxygen becomes depleted in the bottom waters of Devil's Hole. As a consequence, decomposition of organic matter proceeds at a lower rate than if these waters were continuously reoxygenated. Therefore, less CO_2 is being produced from this process, and consequently, less carbonate material is being dissolved (Moulin et al. 1985; Morse and Mackenzie 1990; Burdige and Zimmerman 2002). Thus, it is possible that under future pCO_2 conditions, dissolution rates in typical carbonate environments could actually be significantly higher than those rates estimated in Devil's Hole during the summers of 2004 and 2005.

If one assumes that the density stratification in Devil's Hole had developed by the end of May and lasted until the last day in September (122 days), and the rates of dissolution remained constant throughout this time, the estimated rates of dissolution correspond to a loss in carbonate mass of 87 to 468 g m^{-2} for this time period. Considering the entire area of subthermocline sediments below or at 20 m depth (0.48 km^2), this corresponds to a loss of 42.3 to 224.6 tons of $CaCO_3$. At first this may seem to be substantial, but if one considers the top centimeter of the sediments and assumes a porosity of 80%, the amount of carbonate dissolved corresponds to 1.5 to 8.1% of the total carbonate mass in this sediment layer. According to Thorstenson and Mackenzie (1974), the average sedimentation rate in Devil's Hole has been approximately 70 cm/1000 years based on radiocarbon dating of peat at the base of the sediments, but the rate may be considerably higher at present.

If one were to assume that the derived rates of carbonate dissolution in Devil's Hole are analogous to the rates of dissolution that we may observe in carbonate environments under future high pCO_2 conditions (see previous discussion), extrapolation for an entire year corresponds to a loss in carbonate material of 264 to 1402 grams m^{-2} yr^{-1}. The latter estimate is a significant fraction of current estimates of the average calcium carbonate production of the global coral reef environment (0.6×10^6 km^2; Smith 1978) of about 1500 g m^{-2} yr^{-1} (Milliman 1994; Iglesias-Rodriguez et al. 2002), although local estimates are as high as 2000 to 15000 g m^{-2} yr^{-1} (e.g. Gattuso et al. 1993, 1996, 1999; Bates, 2002). Based on experimental calcification-carbonate saturation state relationships, future projections suggest that calcium carbonate production may decrease by as much as 40% by year 2100 (Buddemeier et al. 2004) and by 85-90% by year 2300 (Andersson et al. 2005). In such a scenario, the upper dissolution estimate of the present study will already exceed carbonate production during the 21st century and the lower estimate will

exceed the estimated production by year 2300. Consequently, net accumulation of carbonate material on coral reefs may already be decreasing owing to rising pCO_2, but at some point in time, all other factors remaining constant, when dissolution of carbonate material exceeds its production, net accumulation will be negative and coral reefs will start to loose carbonate mass.

It has been proposed that increased dissolution of high Mg-calcite minerals could act as a buffer to restore changes to surface seawater pH and carbonate saturation state owing to rising atmospheric CO_2, thereby alleviating any negative effects imposed on marine calcareous organisms (Barnes and Cuff 2000; Halley and Yates 2000). However, despite significant dissolution of high Mg-calcite minerals and production of alkalinity from this process in Devil's Hole, the seawater saturation state with respect to aragonite was sufficiently low according to experimental relationships between carbonate saturation state and calcification rates to affect negatively the rate of calcification of marine calcifiers under similar future conditions (e.g. Gattuso et al. 1999; Langdon et al. 2000; Leclercq et al. 2002). Thus, the observational results of the present study suggest that dissolution of high Mg-calcite will not buffer the surface ocean from changes imposed by rising atmospheric CO_2. Similarly, Andersson et al. (2003, 2005; Morse et al. 2006) concluded based on numerical modeling results that although dissolution of metastable carbonate minerals would increase in the future owing to rising atmospheric CO_2, this process would not produce sufficient alkalinity to buffer the global coastal ocean significantly on time-scales of decades to centuries. Even if the rate of dissolution of shallow water high Mg-calcite minerals were able to keep up with the current oceanic uptake of anthropogenic CO_2 (~2 Gt yr^{-1}), and assuming this rate remained constant, surface ocean pH and aragonite saturation state would remain unchanged for about 60 years before the entire reservoir of reactive Mg-calcite had dissolved (Morse et al. 2006). Consequently, any negative effects on marine

calcifying organisms arising from increasing pCO_2 and decreasing carbonate saturation state will not be resolved by dissolution of metastable carbonate minerals.

6. CONCLUSIONS

Evidences from both seawater chemistry and sediment mineral composition in Devil's Hole, Bermuda, show that high Mg-calcite minerals are preferentially dissolved under conditions of elevated pCO_2 in the natural environment. Estimated rates of dissolution under pCO_2 conditions anticipated by the end of the 21st century and beyond range from 0.3 to 1.6 mmol m^{-2} h^{-1}. On a yearly basis, this range of estimates corresponds to 264 to 1402 grams m^{-2} yr^{-1}, the latter value is close to present day estimates of average global coral reef calcification of 1500 grams m^{-2} yr^{-1}. If the rate of calcification were suppressed by 40% by the end of the 21st century, or 90% by the end of the 23rd century, which has been proposed as a result of rising pCO_2 and decreasing surface seawater carbonate saturation state, net accumulation of carbonate material on coral reefs and in other carbonate dominated ecosystems will at some point in time within the next century or two become negative. Consequently, these environments will be subject to a net loss in carbonate material owing to modifications in surface seawater pH and carbonate saturation state imposed by anthropogenic combustion of fossil fuels and rising atmospheric pCO_2.

APPENDIX

The appendix demonstrates the calculations of excess alkalinity (ΔTA) based on linear regressions of normalized alkalinity profiles (S=36) for each sampling time in Devil's Hole in 2004 and 2005 (Figure 7). Excess alkalinity was calculated by subtracting the pre-formed alkalinity (TA^0) from the total depth integrated alkalinity (ΣTA) over the depth range considered. The pre-formed alkalinity was assumed to equal the average mixed layer alkalinity during the first day of sampling for each year.

Excess alkalinity 08-24-04

$$\Delta TA = \Sigma TA - TA^0 =$$

$$\int_{z_1}^{z_3}[\Sigma TA]dz - \int_{z_1}^{z_3}[TA^0]dz =$$

$$\int_{z_1}^{z_2}[x_2]dz + \int_{z_2}^{z_3}[x_1]dz - \int_{z_1}^{z_3}[TA^0]dz =$$

$$\int_{13.5}^{19.905}\left[\frac{Z+424.44}{191.86}\right]dz + \int_{19.906}^{23.5}\left[\frac{Z+63.204}{35.885}\right]dz - \int_{13.5}^{23.5}[2.2826]dz =$$

0.405 mmol kg^{-1} m = 415 mmol m^{-2}

Excess alkalinity 09-16-04

$$\Delta TA = \Sigma TA - TA^0 =$$

$$\int_{z_1}^{z_4}[\Sigma TA]dz - \int_{z_1}^{z_4}[TA^0]dz =$$

$$\int_{z_1}^{z_2}[x_3]dz + \int_{z_2}^{z_3}[x_2]dz + \int_{z_3}^{z_4}[x_1]dz - \int_{z_1}^{z_4}[TA^0]dz =$$

$$\int_{18.8}^{20.957}\left[\frac{Z+34.352}{23.409}\right]dz + \int_{20.958}^{21.995}\left[\frac{Z+173.98}{82.505}\right]dz + \int_{21.996}^{23.5}\left[\frac{Z-5.9582}{6.7518}\right]dz - \int_{18.8}^{23.5}[2.2826]dz =$$

0.466 mmol kg^{-1} m = 477 mmol m^{-2}

Excess alkalinity 08-02-05

$$\Delta TA = \Sigma TA - TA^0 =$$

$$\int_{z_1}^{z_4}[\Sigma TA]dz - \int_{z_1}^{z_4}[TA^0]dz =$$

$$\int_{z_1}^{z_2}[x_3]dz + \int_{z_2}^{z_3}[x_2]dz + \int_{z_3}^{z_4}[x_1]dz - \int_{z_1}^{z_4}[TA^0]dz =$$

$$\int_{16}^{18.992}\left[\frac{Z+83.367}{43.247}\right]dz + \int_{18.993}^{22.141}\left[\frac{Z+354.64}{157.86}\right]dz + \int_{22.142}^{23.5}\left[\frac{Z+106.24}{53.788}\right]dz - \int_{16}^{23.5}[2.2976]dz =$$

0.487 mmol kg^{-1} m = 499 mmol m^{-2}

Excess alkalinity 08-16-05

$$\Delta TA = \Sigma TA - TA^0 =$$

$$\int_{z_1}^{z_4}[\Sigma TA]dz - \int_{z_1}^{z_4}[TA^0]dz =$$

$$\int_{z_1}^{z_2}[x_3]dz + \int_{z_2}^{z_3}[x_2]dz + \int_{z_3}^{z_4}[x_1]dz - \int_{z_1}^{z_4}[TA^0]dz =$$

$$\int_{16.68}^{20.744}\left[\frac{Z+56.108}{31.892}\right]dz + \int_{20.745}^{22.999}\left[\frac{Z+597.46}{256.54}\right]dz + \int_{23}^{23.5}\left[\frac{Z+22.665}{18.881}\right]dz - \int_{16.68}^{23.5}[2.2976]dz =$$

0.520 mmol kg^{-1} m = 532 mmol m^{-2}

Excess alkalinity 09-06-05

$$\Delta TA = \Sigma TA - TA^0 =$$

$$\int_{z_1}^{z_4}[\Sigma TA]dz - \int_{z_1}^{z_4}[TA^0]dz =$$

$$\int_{z_1}^{z_2}[x_3]dz + \int_{z_2}^{z_3}[x_2]dz + \int_{z_3}^{z_4}[x_1]dz - \int_{z_1}^{z_4}[TA^0]dz =$$

$$\int_{17.75}^{20.039}\left[\frac{Z+9.5278}{12.092}\right]dz + \int_{20.040}^{23.008}\left[\frac{Z+325.45}{141.29}\right]dz + \int_{23.009}^{23.5}\left[\frac{Z+4.1585}{7.6435}\right]dz - \int_{17.75}^{23.5}[2.2976]dz =$$

0.684 mmol kg^{-1} m = 700 mmol m^{-2}

ACKNOWLEDGEMENT

Thank you bla bla bla. This research was funded by grants xxxxxxx.

REFERENCES

Agegian CR (1985) The biogeochemical ecology of *Porolithon gardineri* (foslie). Ph.D. dissertation, University of Hawaii, Honolulu, p. 178.

Alexandersson ET (1976) Actual and anticipated petrographic effects of carbonate undersaturation in shallow seawater. Nature 262:653-657.

Alexandersson ET (1979) Marine maceration of skeletal carbonates in the Skagerrak, North Sea. Sedimentology 26:845-852.

Andersson AJ, Mackenzie FT, Lerman A (2005) Coastal ocean and carbonate systems in the high CO_2 world of the Anthropocene. American Journal of Science 305:875–918.

Andersson AJ, Mackenzie FT, Ver LM (2003) Solution of shallow-water carbonates: An insignificant buffer against rising atmospheric CO_2. Geology 31:513– 516.

Archer D, Kheshgi H, Maier-Reimer E (1998) Dynamics of fossil fuel CO_2 neutralization by marine $CaCO_3$. Global Biogeochemical Cycles 12:259-276.

Balzer W, Wefer G (1981) Dissolution of carbonate minerals in a subtropical shallow marine environment. Marine Chemistry 10:545-558.

Barnes DJ, Cuff C (2000) Solution of reef rock buffers seawater against rising atmospheric CO_2. In: Hopley D, Hopley M, Tamelander J et al (eds) Proceedings of the Ninth International Coral Reef Symposium Abstracts, State Ministry for the Environment, Indonesia, pp. 248.

Barnes DJ, Devereux MJ (1984) Productivity and calciifcation on a coral reef: a survey using pH and oxygen electrode techniques. Journal of Experimental Marine Biology and Ecology 79:213-231.

Bates NR, Michaels AF, Knap AH (1996) Alkalinity changes in the Sargasso Sea: geochemical evidence of calcification? Marine Chemistry 51:347-358.

Bischoff WD, Bertram MA, Mackenzie FT et al (1993) Diagenetic stabilization pathways of magnesian calcites. Carbonates and Evaporites 8:82-89.

Bischoff WD, Mackenzie FT, Bishop FC, (1987) Stabilities of synthetic magnesian calcites in aqueous solution: comparison with biogenic materials. Geochimica et Cosmochimica Acta 51:1413-1423.

Boucher G, Clavier J, Hily C et al (1998) Contribution of soft-bottoms to the community metabolism (primary production and calcification) of a barrier reef flat (Moorea, French Polynesia). Journal of Experimental Marine Biology and Ecology 225:269-283.

Brewer PG, Goldman JC (1976) Alkalinity changes generated by phytoplankton growth. Limnology and Oceanography 21:108-117.

Brown FI (1980) The nitrogen cycle and heat budget of a subtropical lagoon, Devil's Hole, Harrington Sound, Bermuda: Implications for nitrous oxide production and consumption in marine environments. Ph.D. dissertation, Northwestern University, Evanston, Illinois, p. 317.

Brown FI (1978) Mixing processes. In Barnes JA, Bodungen BV (eds) The Bermuda Marine Environment, vol 2, Bermuda Biological Station Spec. Pub. 17, pp. 10-30.

Buddemeier RW, Kleypas JA, Aronson RB (2004) Coral reefs and global climate change: Potential contributions of climate change to stresses on coral reef ecosystems. Report prepared for the Pew Center on Global Climate Change, Arlington, VA, p. 44.

Burdige DJ, Zimmerman RC (2002) Impact of sea grass density on carbonate dissolution in Bahamian sediments. Limnology and Oceanography 47:1751-1763.

Busenberg E, Plummer NL (1989) Thermodynamics of magnesian calcite solid solution-solutions at 25°C and 1 atm total pressure. Geochimica et Cosmochimca Acta 53:1189-1208.

Caldeira K, Wickett ME (2003) Anthropogenic carbon and ocean pH. Nature 425:365.

Chave KE (1954) Aspects of the biogeochemistry of magnesium 1. Calcareous marine organisms. The Journal of Geology 62:266-283.

Chave KE (1962) Factors influencing the mineralogy of carbonate sediments. Limnology and Oceanography 7:218-223.

Chisholm JRM, Gattuso J-P (1991) Validity of the alkalinity anomaly technique for investigating calcification and photosynthesis in coral reef communities. Limnology and Oceanography 36:1232-1239.

Conand C, Chabenet P, Cuet P, Letourneur Y (1997) The carbonate budget of a fringing reef in La Reunion Island (Indian Ocean): Sea urchin and fish bioerosion and net calcification. Proceedings of the Eighth International Coral Reef Symposium 1:953–958.

Denman KL, Gargett AE (1983) Time and space scales of vertical mixing and advection of phytoplankton in the upper ocean. Limnology and oceanography 28:801-815.

Dickson AG (1981) An exact definition of total alkalinity and a procedure for the estimation of alkalinity and total inorganic carbon from titration data. Deep-Sea Research 28A:609-623.

Dickson A, Millero FJ (1987) A comparison of the equilibrium constants for the dissociation of carbonic acid in seawater media. Deep-Sea Research 38:1733-1743.

Dillon TM, Caldwell DR (1980) The batchelor spectrum and dissipation in the upper ocean. Journal of Geophysical Research 85:1910-1916.

DOE (1994) Handbook of methods for the analysis of the various parameters of the carbon dioxide system in sea water; version 2. Dickson AG, Goyet C (eds) ORNL/CDIAC-74.

Feely RA, Sabine CL, Lee K et al (2004) Impact of anthropogenic CO_2 on the $CaCO_3$ system in the oceans. Science 305:362-366.

Garrels RM, Mackenzie FT (eds) (1980) Some aspects of the role of the shallow ocean in global carbon dioxide uptake. Workshop report: Carbon dioxide effects research and assessment program, United States Department of Energy.

Gattuso J-P, Allemand PD, Frankignoulle M (1999) Photosynthesis and calcification at cellular, organismal and community levels in coral reefs: A review on interactions and control by carbonate chemistry. American Zoologist 39:160-188.

Gattuso J-P, Pichon M, Delesalle B et al (1993) Community metabolism and air-sea CO_2 fluxes in coral reef ecosystems (Moorea, French Polynesia). Marine Ecology Progress Series 96:259-267.

Gattuso J-P, Pichon M, Delesalle B et al (1996) Carbon fluxes in coral reefs. I. Lagrangian measurement of community metabolism and resulting air-sea CO_2 disequilibrium. Marine Ecology Progress Series 145:109-121.

Goyet C, Bradshaw AL, Brewer PG (1991) The carbonate system in the Black Sea. Deep-Sea Research 38(Suppl. 2):S1049-1068.

Halley RB, Yates KK (2000) Will reef sediments buffer corals from increased global CO_2. In: Hopley D, Hopley M, Tamelander J et al (eds) Proceedings of the Ninth International Coral Reef Symposium Abstracts, State Ministry for the Environment, Indonesia, pp. 248.

Iglesias-Rodriguez MD, Armstrong R, Feely R et al (2002) Progress made in study of ocean's calcium carbonate budget. EOS, Transactions American Geophysical Union, 83(34):365.

IPCC Intergovernmental Panel on Climate Change (2001) Climate Change 2001: The Scientific Basis—Contribution of Working Group I to the Third Assessment Report of the Intergovernmental Panel on Climate Change. Houghton JT, Ding Y, Griggs DJ et al (eds) Cambridge University Press, New York, p. 881.

Kanamori S, Ikegami H (1980) Computer-processed potentiometric titration for the determination of calcium and magnesium in seawater. Journal of Oceanography 36:177-184.

Kinsey DW (1978) Alkalinity changes and coral reef calcification. Limnology and Oceanography 23:989–991.

Kleypas JA, Buddemeier RW, and Gattuso J-P (2001) The future of coral reefs in an age of global change. International Journal of Earth Sciences (Geologische Rundschau) 90:426-437.

Kleypas JA, Buddemeier RW, Archer D et al (1999) Geochemical consequences of increased atmospheric carbon dioxide on coral reefs. Science 284:118-120.

Kleypas JA, Feely RA, Fabry VJ et al (2006) Impacts of Ocean Acidification on Coral Reefs and Other Marine Calcifiers: A Guide for Future Research, report of a workshop held 18–20 April 2005, St. Petersburg, FL, sponsored by NSF, NOAA, and the U.S. Geological Survey, p. 88.

Knap AH, Michaels AF, Dow RL et al (1993) BATS Methods Manual, Version 3. U.S. JGOFS Planning Office, Woods Hole, MA.

Knap AH, Michaels AF, Steinberg D et al (1997) BATS Methods Manual. U.S. JGOFS Planning Office, Woods Hole.

Langdon C, Takahashi T, Sweeney C et al (2000) Effect of calcium carbonate saturation state on the calcification rate of an experimental coral reef. Global Biogeochemical Cycles 14:639-654.

Leclercq N, Gattuso J-P, Jaubert J (2002) Primary production, respiration, and calcification of a coral reef mesocosm under increased CO_2 partial pressure. Limnology and Oceanography 47:558-564.

Lewis E, Wallace DWR (1998) Program Developed for CO_2 System Calculations. ORNL/CDIAC-105: Carbon Dioxide Information Analysis Center, Oak Ridge National Laboratory, U.S. Department of Energy, Oak Ridge, Tennessee.

Li Y-H (1973) Vertical eddy diffusion coefficient in Lake Zürich. Schweizerische Zeitschrift für Hydrologie 35:1-7.

Mackenzie FT, Agegian CR (1989) Biomineralization and tentative links to plate tectonics. In: Crick RE (ed) Origin, evolution, and modern aspects of biomineralization in plants and animals, Plenum Press, New York, pp. 11-27.

Mackenzie FT, Bischoff WD, Bishop FC et al (1983) Magnesian calcites: Low temperature occurrence, solubility and solid-solution behavior. In: Reeder RJ (ed) Reviews in Mineralogy, Carbonates: mineralogy and chemistry, Mineralogical Society of America, pp. 97-143.

Mackenzie FT, Lerman A, Ver, LM (2001) Recent past and future of the global carbon cycle. In: Gerhard LC, Harrison WE, Hanson BM (eds) Geological Perspectives of Global Climate Change, special publication, Am. Assoc. of Petrol. Geol., Tulsa, Okla. pp. 51– 82.

Mehrbach C, Culberson CH, Hawley JE et al (1973) Measurement of the apparent dissociation constants of carbonic acid in seawater at atmospheric pressure. Limnology and Oceanography 18:897-907.

Morris BJ, Barnes J, Brown F et al (1977) The Bermuda marine environment: a report of the Bermuda inshore waters investigation 1976-1977. Bermuda Biological Station Spec. Pub. 15, p. 120.

Morse JW, Andersson AJ, Mackenzie FT (2006) Initial responses of carbonate-rich shelf sediments to rising atmospheric pCO_2 and ocean acidification: Role of high Mg-calcites. Geochimica et Cosmochimica Acta 70:5814-5830.

Neumann AC (1963) Processes of recent carbonate sedimentation in Harrington sound Bermuda. Ph.D. dissertation, Lehigh University, Betlehem, Pennsylvania, p. 130.

Neumann AC (1965) Processes of recent carbonate sedimentation in Harrington sound Bermuda. Bulletin of Marine Science 15:987-1035.

Orr JC, Fabry VJ, Aumont O et al (2005) Anthropogenic ocean acidification over the twenty-first century and its impacts on calcifying organisms. Nature 437:681–686.

Plummer LN, Mackenzie FT (1974) Predicting mineral solubility from rate data: application to the dissolution of magnesian calcites. American Journal of Science 274:61-83.

Riebesell U, Zondervan I, Rost B et al (2000) Reduced calcification of marine plankton in response to increased atmospheric CO_2. Nature 407:364-367.

Sabine CL, Feely RA, Gruber N et al (2004) The oceanic sink for anthropogenic CO_2. Science 305:367-371.

Schmalz RF, Chave KE (1963) Calcium carbonate: Affecting saturation in ocean waters of Bermuda. Science 139:1206-1207.

Smith SV (1978) Coral-reef area and the contributions of reefs to processes and resources of the world's oceans. Nature 273:225-226.

Smith SV, Kinsey DW (1978) Calcification and organic carbon metabolism as indicated by carbon dioxide. In: Stoddart DR, Johannes RE (eds) Coral reefs: research methods, Monogr. Oceanogr. Methodol., 5, UNESCO.

Thorstenson DC, Mackenzie FT (1974) Time variability of pore water chemistry in recent carbonate sediments, Devil's Hole, Harrington Sound, Bermuda. Geochimica et Cosmochimica Acta 38:1-19.

Walter LM, Burton EA (1990) Dissolution of recent platform carbonate sediments in marine pore fluids. American Journal of Science 290:601-643.

Wollast R, Garrels RM, Mackenzie FT (1980) Calcite-seawater reactions in ocean surface waters. American Journal of Science 280:831-848.

Yates KK, Halley RB (2003) Measuring coral reef community metabolism using new benthic chamber technology. Coral reefs 22:247-255.

Yates KK, Halley RB (2006) CO_3^{2-} concentration and pCO_2 thresholds for calcification and dissolution on the Molokai reef flat, Hawaii. Biogeosciences, 3:357-369.

Zeebe RE, Wolf-Gladrow D (2003) CO_2 in Seawater: Equilibrium, Kinetics, Isotopes. Elseiver, Amsterdam, p. 346.

FIGURE CAPTIONS

Figure 1. Map of Harrington Sound, Bermuda. Flatts inlet (F.I.) is shown by the arrow and the location of Devil's Hole (D.H.) is marked by a star.

Figure 2. Vertical profiles of temperature and pCO_2 in Devil's Hole at or close to the timing of the maximum stratification of the seasonal thermocline (September 6, 2005) as well as after the overturn of the thermocline (September 27, 2005). The pCO_2 of the subthermocline water is significantly higher than what is normally observed in natural shallow surface seawater environments.

Figure 3. Water column physiochemical properties of Devil's Hole, Bermuda, during August and September of 2004 and 2005, showing temperature (T), salinity (S), density (ρ), dissolved inorganic carbon (DIC), total alkalinity (TA), and dissolved oxygen (DO). Thermally driven density stratification of the water column is clearly visible in the temperature and density profiles. DIC and TA data marked by a dashed symbol indicates that the samples were anoxic and contained H_2S, which precipitated out as HgS (s) upon addition of $HgCl_2$ (aq). The loss in alkalinity accompanying this reaction has not been accounted for in the data shown here.

Figure 4. Temperature-salinity plots of Devil's Hole in the summer of 2004 and 2005. The warm surface mixed layer is easily distinguished from the cold subthermocline layer at each date.

Figure 5. Water column pH_{tot}, pCO_2 and aragonite saturation state in Devil's Hole, Bermuda. Because of thermal density stratification, microbial remineralization of organic matter in the hypolimnion produces CO_2 that increases the pCO_2 and decreases pH and carbonate saturation state analogous to those changes imposed on the surface ocean owing to absorbtion of anthropogenic CO_2 (ocean acidification).

Figure 6. A) Calcium concentration and B) total alkalinity as a function of depth in Devil's Hole on September 16, 2004. The subthermocline layer is shown by the shaded area. C) Normalized calcium concentration (N-[Ca^{2+}]; S=36) as a function of normalized total alkalinity (N-TA) in Devil's Hole in September 1978 and 2004. The straight lines show the predicted theoretical slopes if the average composition of the dissolving mineral phase was pure calcite or aragonite (0 mol% $MgCO_3$), 15 mol% Mg-calcite, or 30 mol% Mg-calcite. Error bars indicate the average 1σ precision of triplicate samples (n=5). See Figure 3 for an explanation on the dashed symbols.

Figure 7. Total alkalinity profiles of Devil's Hole in 2004 and 2005. Linear regressions were used in order to integrate and estimate the excess alkalinity present in the hypolimnion on each date (see Methodology and Appendix). Changes in excess alkalinity between consecutive sampling dates were used together with estimates of diffusive alkalinity flux to derive rates of carbonate dissolution. See Figure 3 for an explanation on the dashed symbols.

Figure 8. A) Relative carbonate composition of surface sediments in Harrington Sound, Bermuda, with respect to aragonite (dark gray), low Mg-calcite (light gray), and high Mg-calcite minerals (black), as a function of grain size (top x-axis) and depth (bottom x-axis). B) Weight percent high Mg-calcite grouped into shallow (8.4±3.0), intermediate (16.9±0.9), or deep sediments (21.5±1.8). For silt and clay sized sediments, the high Mg-calcite composition is significantly less in deep and intermediate sediments than in shallow sediments. C) Mode mol% $MgCO_3$ of 2nd calcite peak (bimodal Mg-calcite composition) observed from XRD analyses as a function of depth. All the data are adopted from Neumann (1963, 1965).

Table 1. Eddy diffusion coefficients calculated from equation (3) based on density data during the summers of 2004 and 2005

	Eddy diffusion coefficients, k_z 10^{-6} m^2 s^{-1}				
Depth (m)	2004-08-24	2004-09-16	2005-08-02	2005-08-16	2005-09-06
17	-	4.4	2.2	2.5	5.5
18	5.0	4.8	1.8	1.7	3.3
19	-	6.1	1.3	1.1	0.9
20	6.2	2.4	-	1.9	1.9
21	-	2.1	-	2.2	1.7
22	2.0	3.0	2.0	10.9	2.1
23	-	0.7	2.1	4.2	2.7
23.5	2.4	1.6	-	2.0	3.2

Table 2. Calculated excess alkalinity, range of vertical alkalinity diffusion, and rate of dissolution in subthermocline waters of Devil's Hole during August and September 2005

Date	Integration depths	Excess alkalinity mmol m^{-2}	Δ Excess alkalinity mmol m^{-2} h^{-1}	Vertical alkalinity diffusion (mmol m^{-2} h^{-1})		Rate of dissolution (mmol m^{-2} h^{-1})	
				Min	Max	Min	Max
24-aug-2004	13.5-23.5	415	-	0.23	0.70	-	-
	13.5-22.0	242	-				
16-sep-2004	18.8-23.5	477	0.11	0.31	0.94	0.14	0.94
	18.8-22.0	166	-0.14				
2-aug-2005	16.0-23.5	499	-	0.17	0.52	-	-
	16.0-23.0	440	-				
16-aug-2005	16.7-23.7	532	0.10	0.23	0.68	0.29	0.70
	16.7-23.0	469	0.09				
6-sep-2005	17.8-23.5	700	0.33	0.60	1.81	0.68	1.58
	17.8-23.0	601	0.26				

Table 3. Carbonate dissolution rates reported from carbonate environments and mesocosms (modified from Kleypas et al., 2006)*

Location	Environment	Dissolution rate mmol m^{-2} h^{-1}	Reference
Bahamas	Ooithic sand	0.01	Burdige et al., 2002
Bahamas	Seagrass	0.04	"
Bermuda	Carbonate sediments	0.3-1.6	This study
Biosphere 2	Hi Mg-calcite sediments	0.2	Langdon et al., 2000
Florida	Patch reef, 10% coral cover	0.5	Yates and Halley, 2003
Florida	Patch reef, top	0.1	"
Florida	Seagrass	0.4	"
Florida	Sand bottom	0.3	"
Florida	Seagrass, red algae	0.4	Walter and Burton, 1990
Florida	Mangrove, red algae	0.8	"
Great Barrier Reef	Reef flat	4	Barnes and Devereux, 1984
Great Barrier Reef	Back reef zone	3	Kinsey, 1978
Hawaii	Patch reef, 22% coral cover	1.5	Yates and Halley, 2003
Hawaii	Patch reef, 10% coral cover	1.1	"
Hawaii	Coral rubble	1.2	"
Hawaii	Sand bottom	0.3	"
Monaco mesocosm	Sand community	0.8	Leclercq et al., 2002
Moorea	Sandy bottom reef flat and lagoon	0.8	Boucher et al., 1998
Reunion Island	Back reef zone	7	Conand et al., 1997

*The results from the present study and those results of Burdige and Zimmerman (2002) has been added to this table

Figure 1.

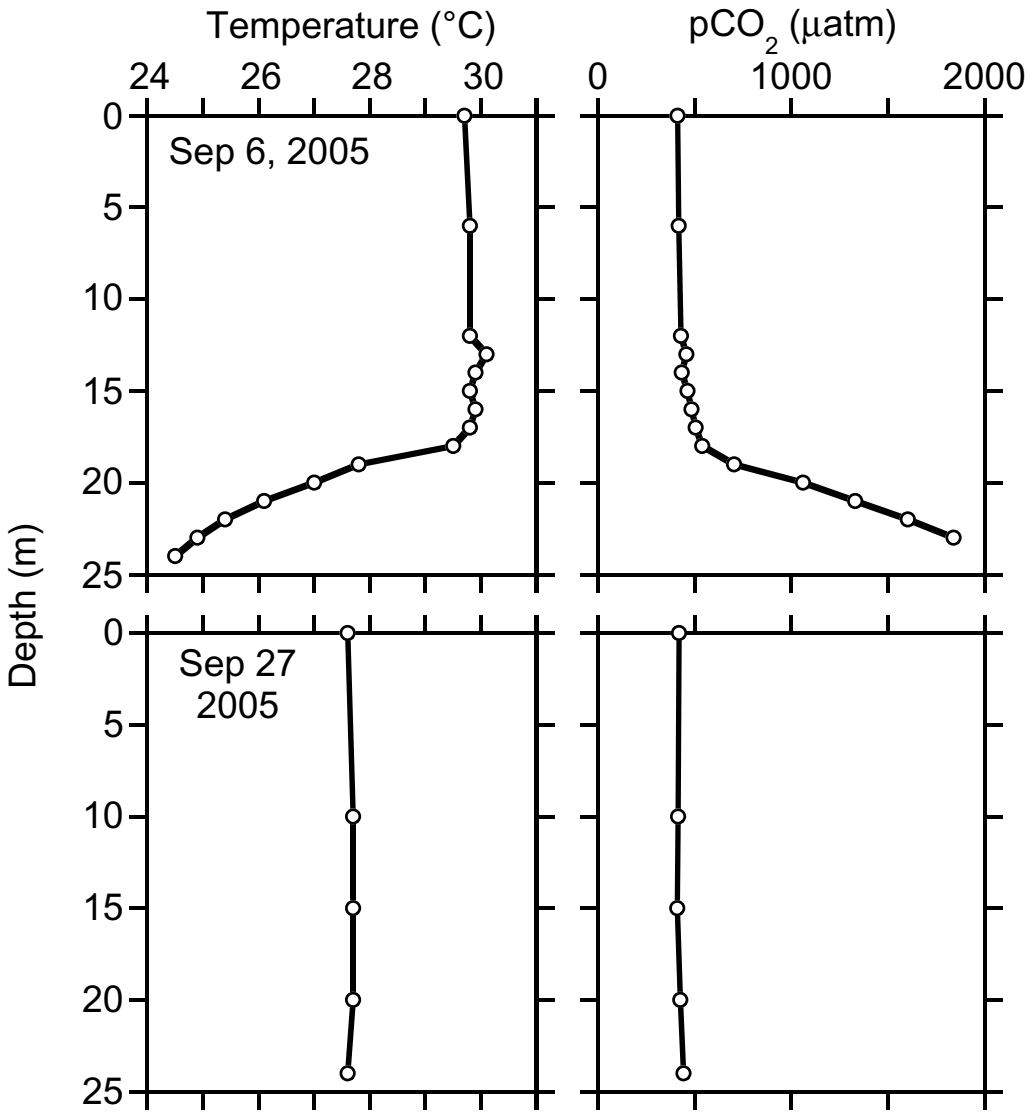
Temperature (°C)
24
26
28
30
pCO2 (µatm)
0
1000
2000
Depth (m)
0
5
10
15
20
25
Sep 6, 2005
Sep 27
2005

Figure 2

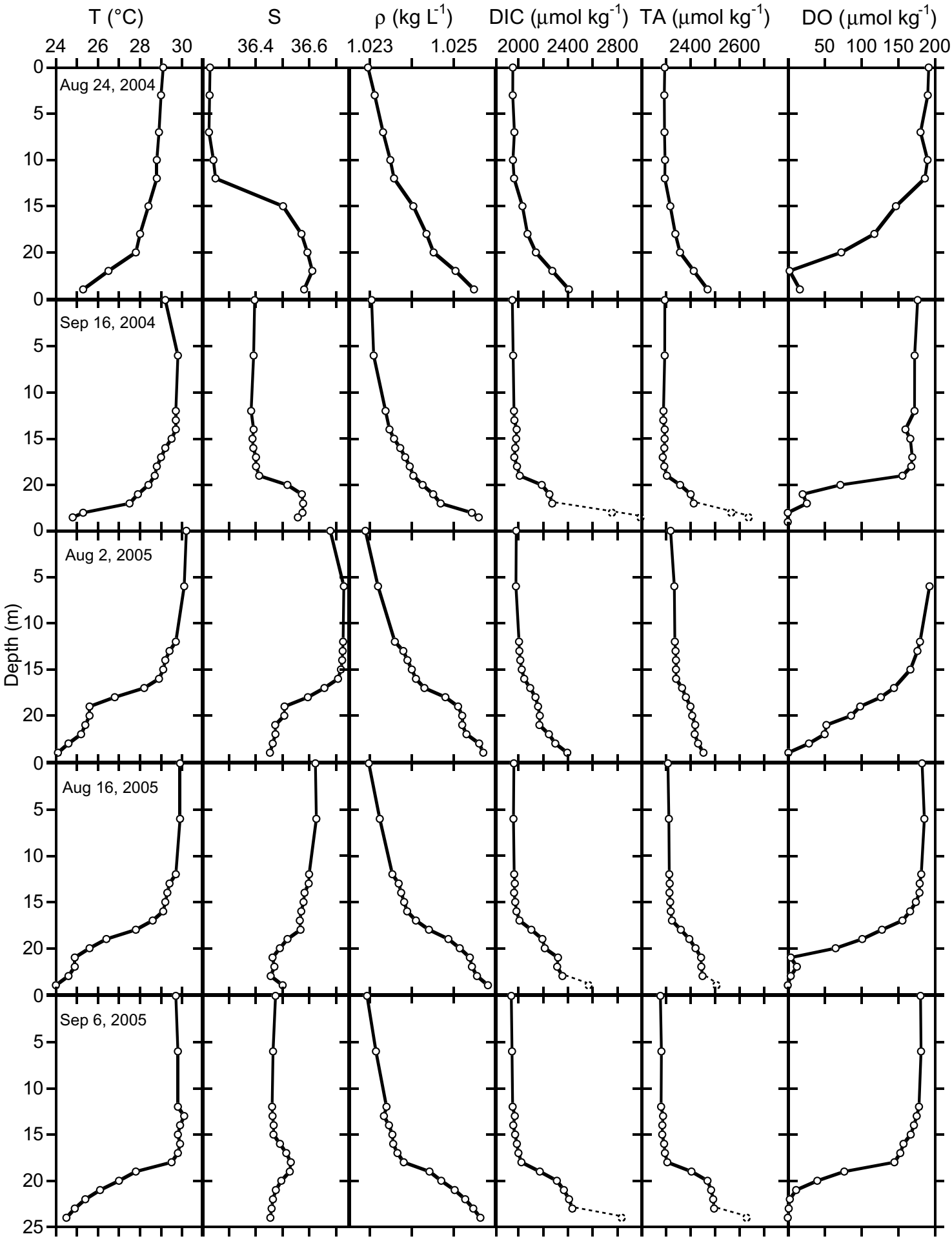
T (°C)
S
ρ (kg L-1)
DIC (µmol kg-1)
TA (µmol kg-1)
DO (µmol kg-1)
24 26 28 30
36.4 36.6
1.023 1.025
2000 2400 2800
2400 2600
50 100 150 200
Aug 24, 2004
Sep 16, 2004
Aug 2, 2005
Aug 16, 2005
Sep 6, 2005
Depth (m)
0 5 10 15 20 25

Figure 3

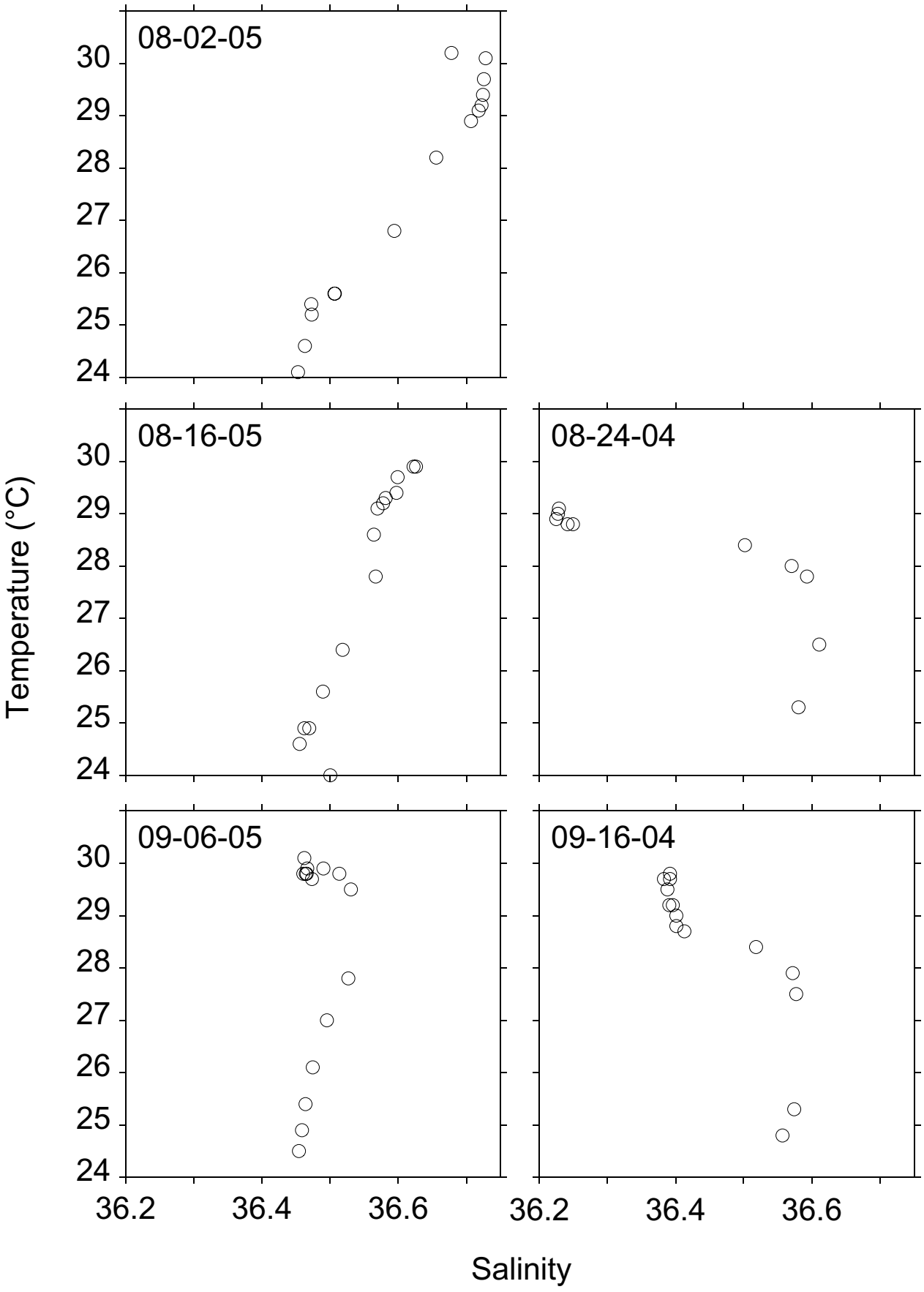
08-02-05
08-16-05
08-24-04
09-06-05
09-16-04
Temperature (°C)
Salinity
30
29
28
27
26
25
24
36.2
36.4
36.6

Figure 4

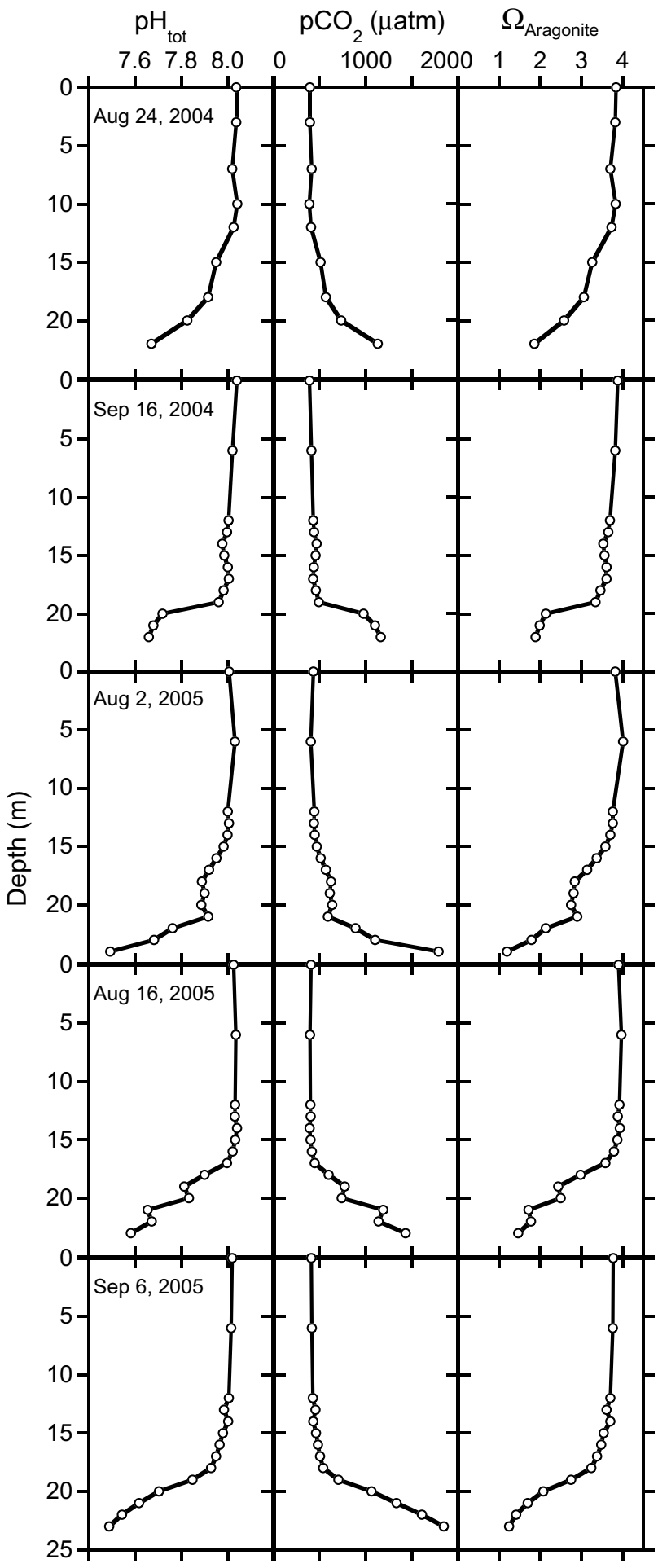
pH tot
pCO 2 (µatm)
Ω Aragonite
7.6 7.8 8.0
0 1000 2000
1 2 3 4
Aug 24, 2004
Sep 16, 2004
Aug 2, 2005
Aug 16, 2005
Sep 6, 2005
Depth (m)
0 5 10 15 20 25

Figure 5

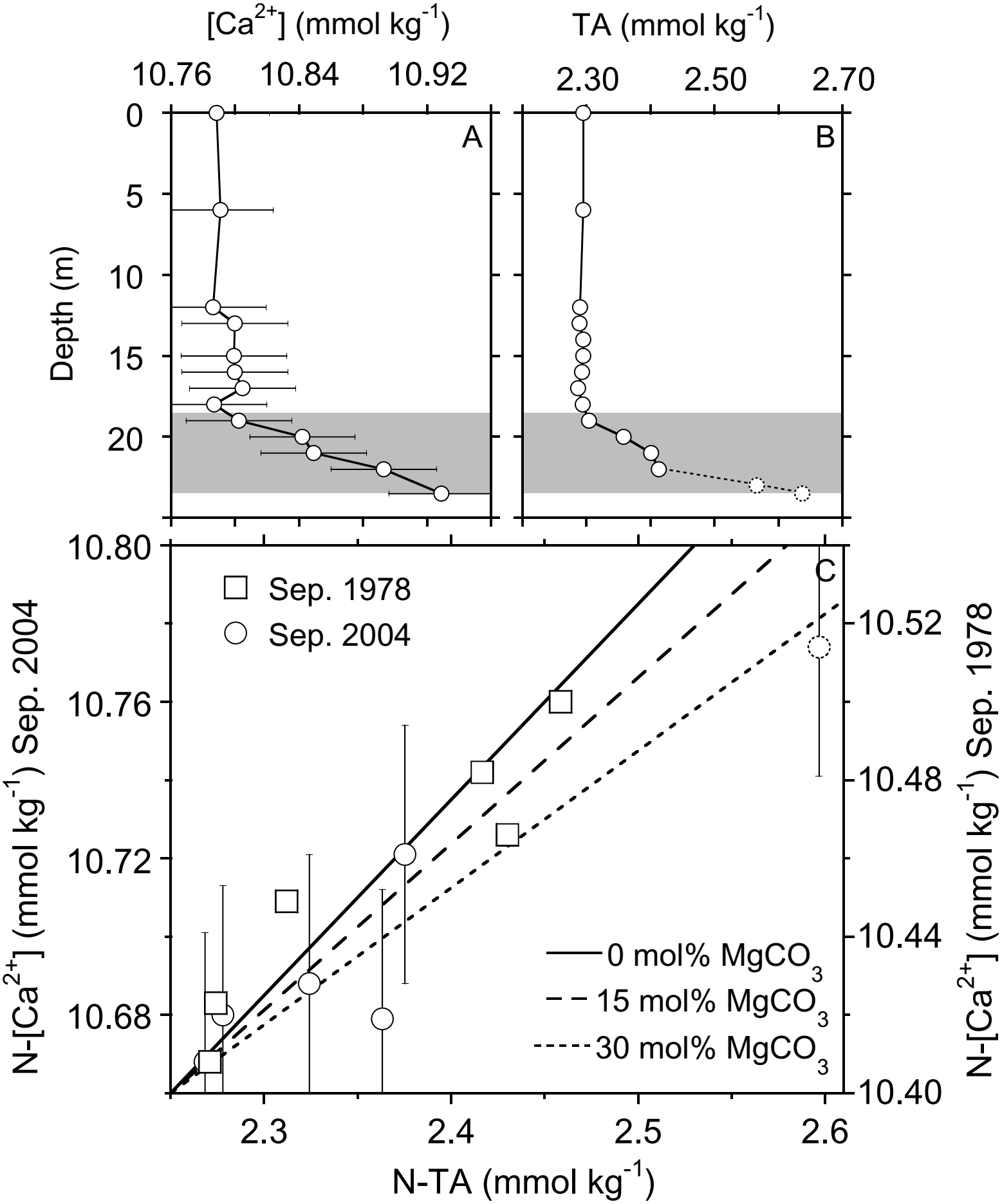
[Ca2+] (mmol kg-1)
TA (mmol kg-1)
10.76
10.84
10.92
2.30
2.50
2.70
A
B
C
Depth (m)
0
5
10
15
20
Sep. 1978
Sep. 2004
0 mol% MgCO3
15 mol% MgCO3
30 mol% MgCO3
N-[Ca2+] (mmol kg-1) Sep. 2004
N-[Ca2+] (mmol kg-1) Sep. 1978
N-TA (mmol kg-1)
10.80
10.76
10.72
10.68
10.52
10.48
10.44
10.40
2.3
2.4
2.5
2.6

Figure 6

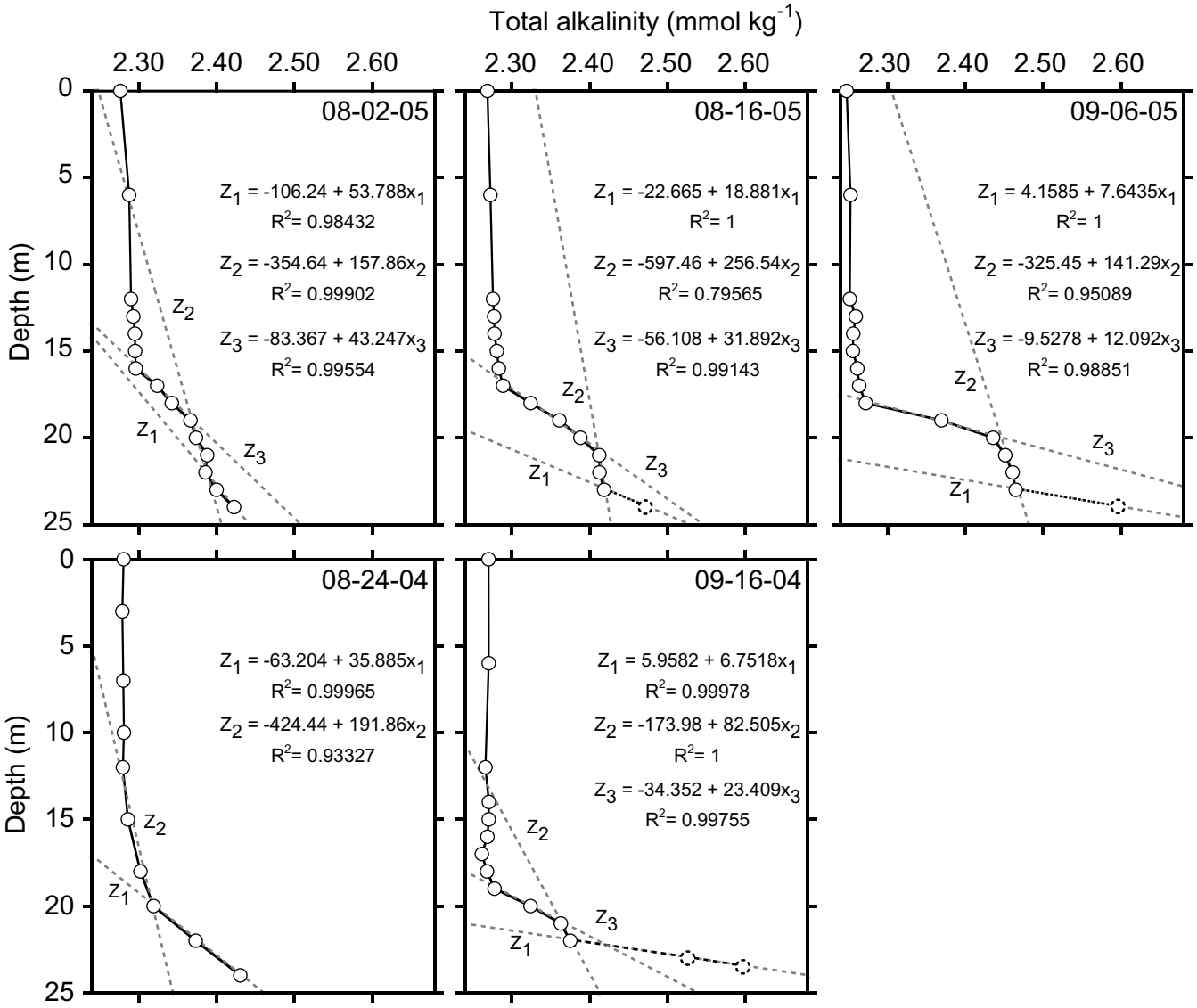
Total alkalinity (mmol kg-1)
2.30
2.40
2.50
2.60
Depth (m)
0
5
10
15
20
25
08-02-05
Z1 = -106.24 + 53.788x1
R2= 0.98432
Z2 = -354.64 + 157.86x2
R2= 0.99902
Z3 = -83.367 + 43.247x3
R2= 0.99554
08-16-05
Z1 = -22.665 + 18.881x1
R2= 1
Z2 = -597.46 + 256.54x2
R2= 0.79565
Z3 = -56.108 + 31.892x3
R2= 0.99143
09-06-05
Z1 = 4.1585 + 7.6435x1
R2= 1
Z2 = -325.45 + 141.29x2
R2= 0.95089
Z3 = -9.5278 + 12.092x3
R2= 0.98851
08-24-04
Z1 = -63.204 + 35.885x1
R2= 0.99965
Z2 = -424.44 + 191.86x2
R2= 0.93327
09-16-04
Z1 = 5.9582 + 6.7518x1
R2= 0.99978
Z2 = -173.98 + 82.505x2
R2= 1
Z3 = -34.352 + 23.409x3
R2= 0.99755

Figure 7

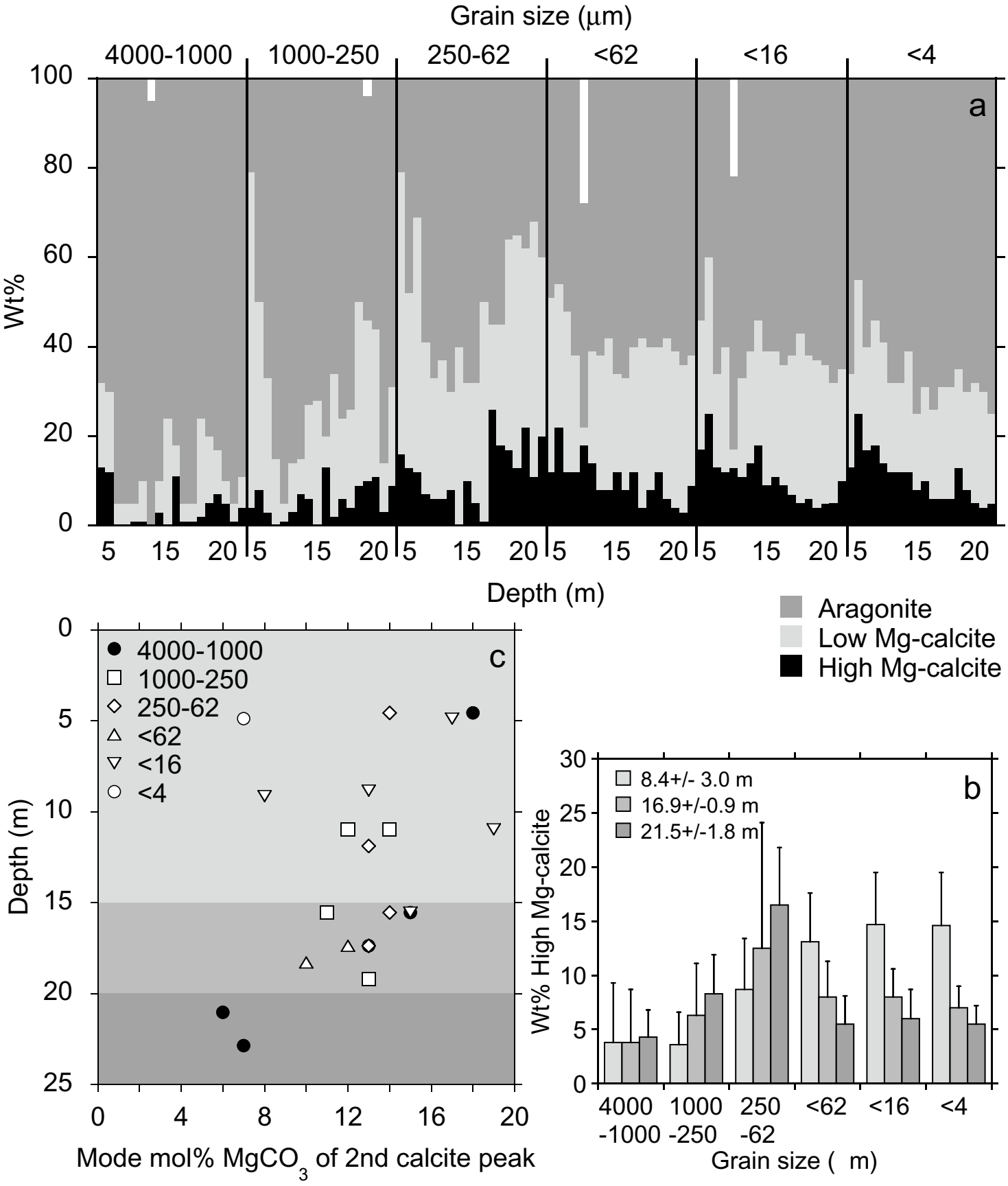
Grain size (μm)
4000-1000
1000-250
250-62
<62
<16
<4
a
Wt%
Depth (m)
Aragonite
Low Mg-calcite
High Mg-calcite
c
4000-1000
1000-250
250-62
<62
<16
<4
Depth (m)
Mode mol% MgCO3 of 2nd calcite peak
b
8.4+/- 3.0 m
16.9+/-0.9 m
21.5+/-1.8 m
Wt% High Mg-calcite
4000 -1000
1000 -250
250 -62
<62
<16
<4
Grain size (m)

Figure 8